Heliyon 9 (2023) e22158

Contents lists available at ScienceDirect

Heliyon

journal homepage: www.cell.com/heliyon

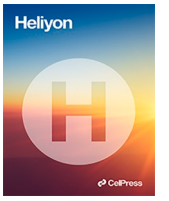

# SERS detection of 1,4-bis(2-aminoethyl)piperazine functionalized GO (AEP-GO) on X60 carbon steel surface in 15% HCl solution

Kabiru Haruna [a,*], Tawfik A. Saleh [a,b], Ahmad A. Sorour [a]

[a] Interdisciplinary Research Center for Advanced Materials, King Fahd University of Petroleum & Minerals, Dhahran, 31261, Saudi Arabia
[b] Department of Chemistry, King Fahd University of Petroleum & Minerals, Dhahran, 31261, Saudi Arabia

ARTICLE INFO

*Keywords:*
SERS
AEP-GO
AgNPs sensor
TEM
DFT

ABSTRACT

In this study, a silver nanoparticle anchored transparent tape sensor was used to detect 1,4-bis(2-aminoethyl)piperazine functionalized GO (AEP-GO) adsorbed on carbon steel surface utilizing the surface-enhanced Raman scattering (SERS) technique. SERS detection enabled the extreme amplification of Raman signals emitted by inhibitor molecules in order to describe their adsorption behavior on metallic/alloy surfaces. The strong corrosion inhibition performance of AEP-GO against carbon steel corrosion in 15 % HCl solution was proven by weight loss, electrochemical measurements and surface characterization techniques in a previous study. The SERS analysis showed the Raman peaks intensity of AEP-GO on the carbon surface gradually increases with increasing AEP-GO concentration. The increasing intensity with concentration correlated well with the previously reported weight loss and electrochemical results. DFT calculation was also carried out to understand the nature of interaction between the adsorbed AEP-GO molecules and the silver nanoparticles. The AEP-GO_Ag adduct's optimized structure reveals the silver metals approached the oxygen atom at the GO epoxy group in AEP-GO rather than the oxygen atoms at the carbonyl and hydroxyl groups. With no restrictions on substrate materials, the fabricated SERS sensor created in this study can be employed as a versatile sensor to characterize corrosion adsorption processes on metal surfaces.

## 1. Introduction

The characterization of corrosion inhibitors can provide a wealth of information about inhibitors' adsorption process and the mode of interaction between metal surfaces and inhibitor molecules. This can aid in a better understanding of how inhibitors work. Weight loss measurement [1,2], electrochemical techniques [3–5], X-ray photoelectron spectroscopy [6–8], SEM/EDS [9,10] time of flight secondary ion mass spectrometry (ToF-SIMS) [11,12], FTIR [3,13], and Raman spectroscopy [14,15] have all been employed to characterize inhibitors. Raman spectroscopy is one of these technologies that can provide a lot of molecular vibration information for molecule identification [16,17], and it's good because it's non-destructive, highly efficient, easy to use, and cheap. Raman signals are however, weak as very few percentage of the photons that hit on sample surfaces (approximately one in a million) can cause the inelastic Raman scattering of light [16,18] that leads to Raman signals. Surface-enhanced Raman scattering (SERS) is a more advanced kind of Raman scattering. It is now a hotbed of interest in the field of nanotechnology and science. When compared to conventional Raman spectroscopy, spectral intensities in SERS are greatly increased (by millions of times or more) [19]. SERS is being employed as a

* Corresponding author.
*E-mail address:* kabiru.haruna@kfupm.edu.sa (K. Haruna).

https://doi.org/10.1016/j.heliyon.2023.e22158
Received 15 April 2023; Received in revised form 26 October 2023; Accepted 6 November 2023
Available online 10 November 2023

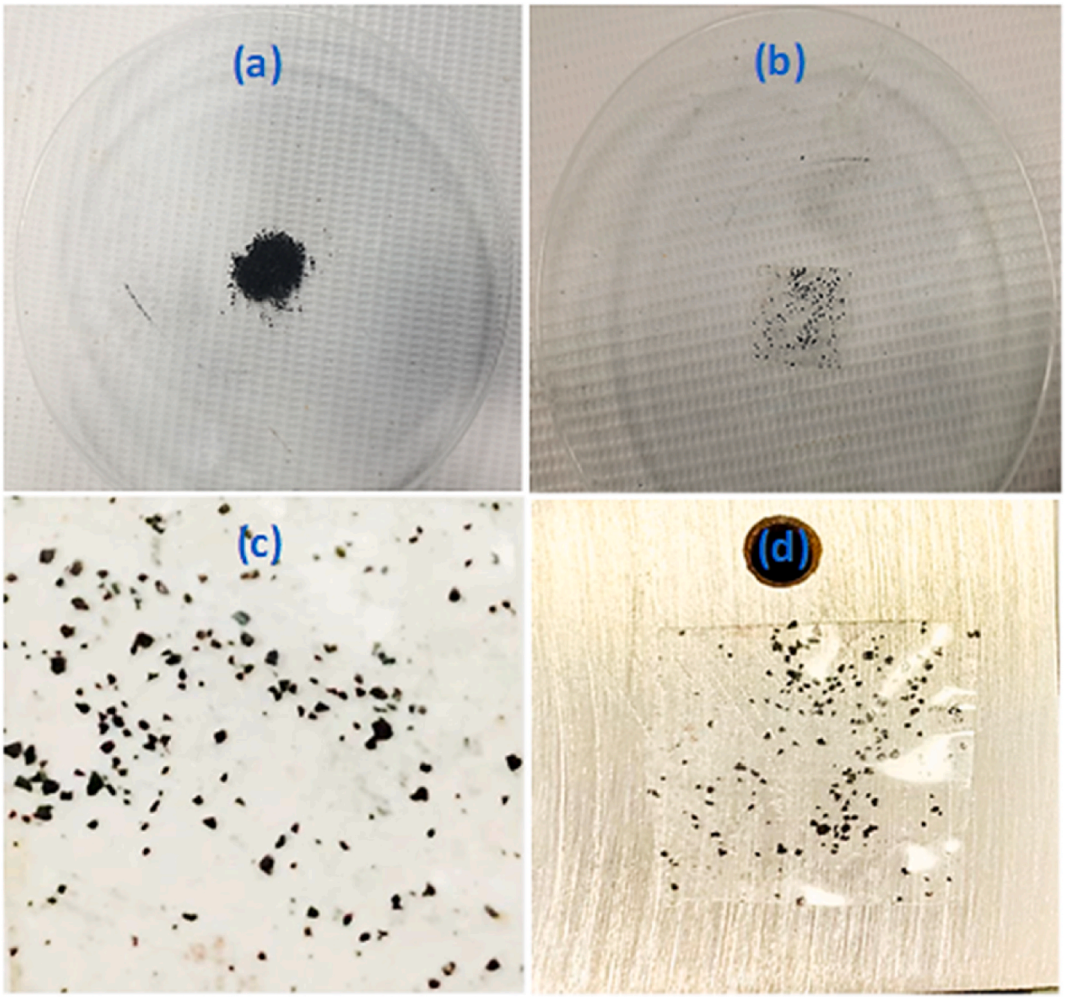


**Fig. 1.** Preparation of SERS tape sensor (a) array of AgNPs (b) transparent adhesive tap pressed in an array of AgNPs (c) fabricated SERS sensor and (d) SERS sensor pasted on carbon steel surface.

successful characterization technique in a variety of fields, including environmental applications, due to its remarkable sensitivity and selectivity. Detection limits as low as femtogram have been observed for some chemical species under certain conditions [20–23]. In today's scientific community, single-molecule detection with SERS is no longer a myth. The electromagnetic interaction of light with metals, which results in significant amplifying effects of the laser field through excitations commonly referred to as Plasmon resonances, is the primary mechanism by which the signals in SERS are amplified. As a surface spectroscopy method, SERS requires that the molecules being detected be on (or near) the metal surface [24].

In recent years, high-resolution detection of corrosion inhibitors using SERS spectroscopy has received attention [25–28]. SERS measurement, in comparison to conventional Raman spectroscopy, has a large signal magnification (ten million) and minimal background signals, thus, allowing for the sensitive detection of corrosion inhibitor compounds. SERS measurements, on the other hand, necessitate SERS active substrates, that is, substrates that exhibit substantial electromagnetic amplification following excitation. The SERS approach has mostly been used to examine corrosion inhibitors on materials that are plasmonic such as gold, silver, and copper [26,28–32]. Ma et al. [33] used a translucent adhesive tape embellished with silver nanoparticles as a SERS sensor to detect benzotriazole inhibitor molecules adsorbed to an aluminum alloy substrate (a non-SERS active substrate) that was immersed in 3.5 % NaCl solution for 72 h by covering the surface of the corroded aluminum alloy with the silver nanorods based tape.

Here we employed SERS using silver nanoparticles (AgNPs) synthesized at room temperature by the reduction of silver nitrate with hydroxylamine hydrochloride to identify adsorbed inhibitor molecules on carbon steel (a non-plasmonic material) surface for the first time and their adsorption behavior as a function of concentration.

## 2. Methodology

### 2.1. Experimental

#### 2.1.1. Materials

Silver nitrate, hydroxylamine hydrochloride, sodium hydroxide, AEP-GO, HCl, waste graphite powder, transparent adhesive tape, and X60 carbon steel. All the chemicals were purchased from Sigma Aldrich except for the graphite powder which was purchased from Fisher Scientific.

#### 2.1.2. Synthesis of AEP-GO

In our prior work, the synthesis and characterization of AEP-GO were discussed [34]. The graphite powder was first purified by adding 1.2 g of $K_2S_2O_8$, 1.2 g of $P_2O_5$, and 2 g of natural graphite powder to 50 ml of $H_2SO_4$ while being stirred at 750 rpm in an ice-water bath. The mixture was then heated to 80 °C in an oil bath. After 4.5 h, the mixture was washed severally with distilled water to attain a pH of 7 and then centrifuged. The obtained purified graphite powder was then dried in a vacuum dryer. The purified graphite powder was used in the synthesis of GO using the modified Hummers' method as described in a previous study [13]. AEP-GO was synthesized by dissolving 0.5g of GO in 200 ml DMF under ultra-sonication. Then, 10 ml of $SOCl_2$ was added. The system was closed and nitrogen gas was purged continuously into the mixture under reflux and stirring for 12 h at 80 °C. The resulting acyl chloride-grafted GO was then centrifuged and separated. The substance was then added to a 500 ml, 3 mg/ml solution of 1,4-piperazinediethylamine in DMF. The mixture was then agitated for one day at 80 °C to allow for a full reaction. After which, it was freeze-dried to obtain the solid AEP-GO.

#### 2.1.3. Synthesis of silver nanoparticles (AgNPs)

The silver colloid was synthesized as described in Ref. [35]. In a nutshell, 10 mL of $1.5 \times 10^{-2}$ M aqueous hydroxylamine hydrochloride was mixed with 10 ml of $3 \times 10^{-2}$ M NaOH before being added to 180 ml of 1.11 $10^{-3}$ M aqueous $AgNO_3$ with stirring. For 20 min at room temperature, the colloidal solution was constantly stirred. The colloid was centrifuged at 10000 rpm and the mother liquor was discarded while the sediment (the silver nanoparticles) was dried in the open air.

#### 2.1.4. Characterization of silver nanoparticles (AgNPs)

The produced silver nanoparticles were characterized using the UV–Vis, TEM, and Raman techniques. The UV–visible spectrum of the colloid was measured at room temperature using a Carr 100 series UV–Visible spectrophotometer (Agilent Technologies) with a standard quartz cuvette within a 350–800 nm range. The stock silver colloid solution was diluted 5 times with distilled deionized water to create the colloid sample. The Raman spectra were obtained using the LabRAM Horiba Raman spectrophotometer at a laser excitation wavelength of 633 nm (50 %), a 50× objective lens, a 600 gr/mm gratings, an acquisition of 60s and a 2s accumulation. A JEOL field emission electron microscope, model JEM-2100F was used to capture the TEM images of the silver nanoparticles.

#### 2.1.5. Silver nanoparticle (AgNPs) sensor fabrication

The AgNPs sensor (Fig. 1c) was fabricated using a translucent adhesive tape. The AgNP sensor was created by placing the translucent adhesive tape and pressing it on a measured amount of array of AgNPs in a watch glass (Fig. 1a & b). The AgNPs array were then moved from the watch glass to the tape after the tape was peeled off.

#### 2.1.6. SERS detection

The carbon steel coupons immersed in different concentrations of AEP-GO (1, 5, 10, 15, 20 & 25 ppm) were removed after 24 h, air-dried and Raman signal was collected in the absence of the AgNPs sensor, and when the fabricated sensor was pasted on the steel coupon surfaces. The SERS signal was collected from the pasted area of the steel substrate (Fig. 1d) using the LabRAM Horiba Raman spectrophotometer at a 60s acquisition, an accumulation of 2s, and a grating of 600 gr/mm.

### 2.2. Computational

Gaussian 09 [36] software was employed to perform the theoretical calculation using DFT at the B3LYP level of theory with the 6-31G and SDD basis sets to examine the nature of the interaction between AEP-GO and Ag by optimizing and evaluating the structure of the AEP-GO_Ag adduct using a Four-Ag cluster as the most probable adsorption site. For the C, N, O, and H atoms, the 6-31G basis sets were utilized, while the SDD was used for the Ag cluster. Of all the DFT types, the B3LYP hybrid functional is the most commonly used for organic molecules and corrosion inhibition studies [37].

## 3. Results & discussion

### 3.1. AgNPs characterization

Average particle sizes are revealed by the colloidal solution's measured UV–visible spectrum's absorption maximum, while particle dispersion may be estimated using the measured UV–visible spectrum's full width at half maximum (fwhm). Fwhm values greater than 100 nm denote polydispersed silver nanoparticles, whereas Fwhm values below 100 nm denote monodispersed silver nanoparticles

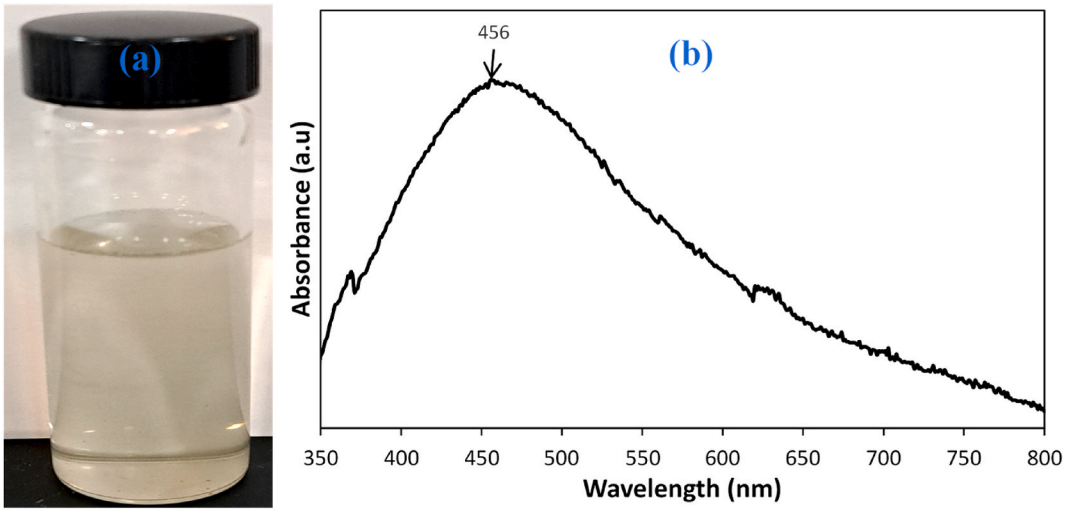


**Fig. 2.** (a) Silver AgNPs colloids (b) UV–Visible Spectrum of the AgNPs.

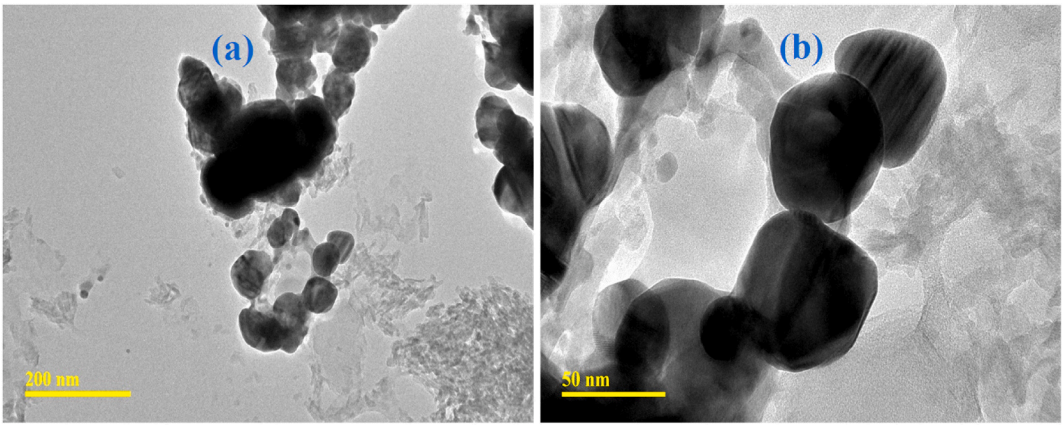


**Fig. 3.** (a) Low and (b) high magnifications TEM micrographs of AgNPs.

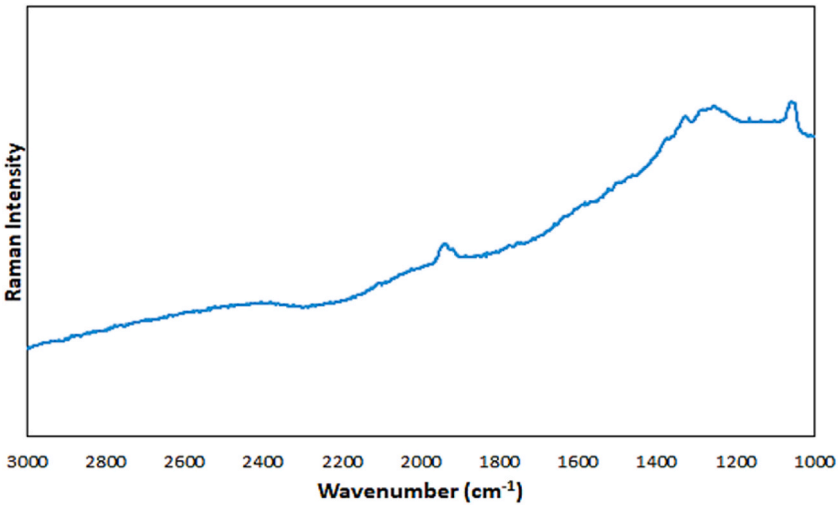


**Fig. 4.** Raman spectrum of the AgNPs.

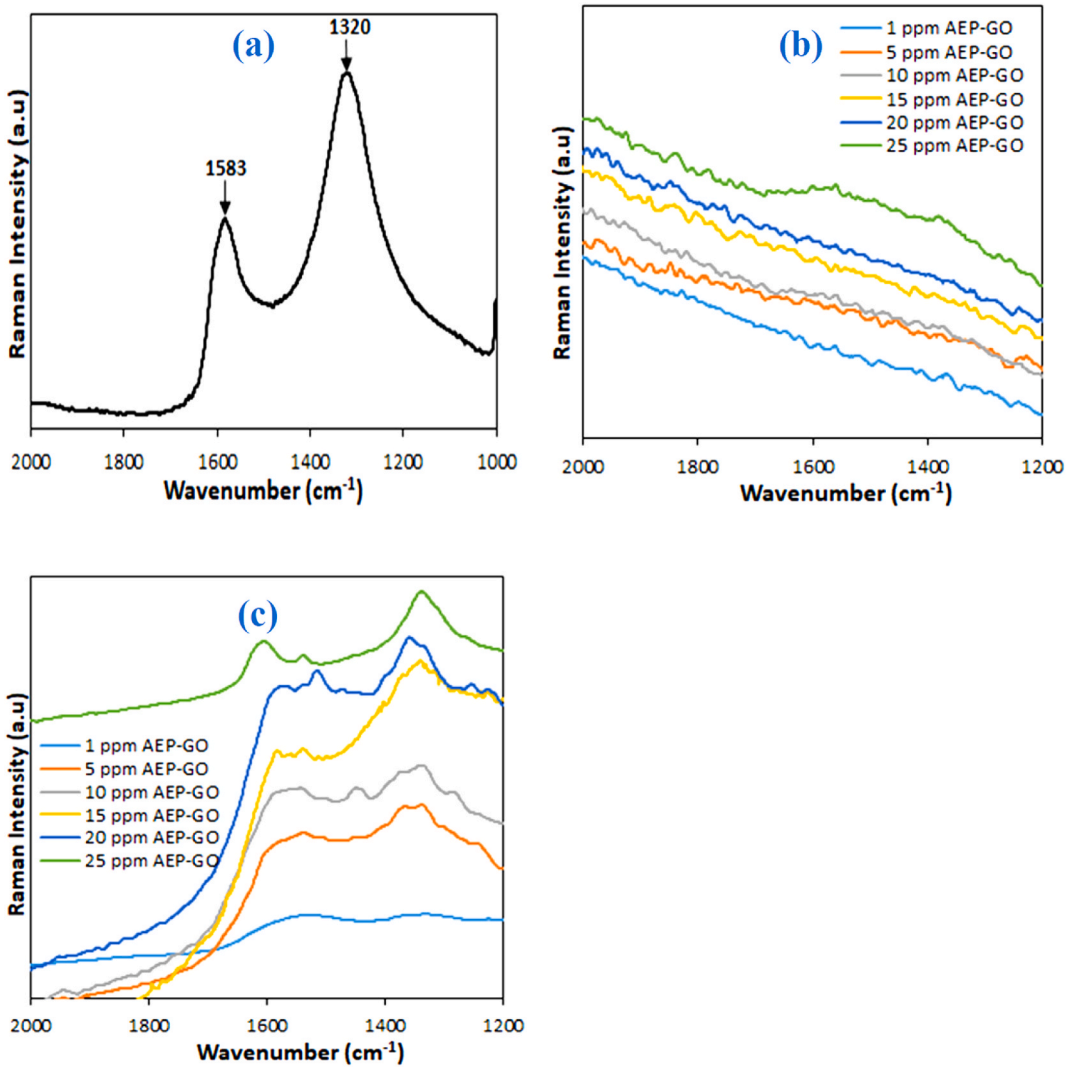


**Fig. 5.** Raman spectra of (a) AEP-GO, (b) AEP-GO protected carbon steel without the SERS sensor and (c) AEP-GO protected carbon steel pasted with the SERS sensor.

[35,38]. The absorption maximum of the silver nanoparticles was observed at 456 nm with a large fwhm extending beyond 100 nm (Fig. 2b). This is indicative of poly-dispersed nanoparticles. The dispersed silver nanoparticles (colloid) was observed to be milky grey (Fig. 2a) similar to that reported by Leopold and Lendl [35].

The low and high magnifications of the AgNPs are shown in Fig. 3a and b respectively. The TEM micrographs support the observation in the UV–visible spectrum. The average particle size of the silver particles could be observed to be roughly 70 nm (Fig. 3), confirming the large size of the particles. The large particle size is a consequence of the dropwise addition of the reducing agent to the silver nitrate. As the reducing agent is added dropwise, the silver particles are likely to increase in size as a consequence of a seeding effect [35]. The silver nanoparticles were observed to be predominantly spherical.

The Raman spectrum of the silver nanoparticles (Fig. 4) shows no noticeable peak in the 1000–3000 $cm^{-1}$ region of the spectrum, except for a weak peak around the 1900 $cm^{-1}$ of the spectrum.

### *3.2. SERS detection of AEP-GO adsorbed on the carbon steel surface*

Normal Raman spectra were collected for the bare inhibitor (AEP-GO) and the steel surfaces immersed in different concentrations of the inhibitor in the absence of the AgNPs sensor. AEP-GO showed characteristics Raman peaks at 1320 & 1583 $cm^{-1}$ (Fig. 5a) corresponding to the D & G-bands respectively of a typical graphitic structure. The steel surfaces showed no visible Raman peaks in the absence of the AgNPs sensor (Fig. 5b). For the corroded steel surfaces pasted with the AgNPs sensor, the characteristics Raman peaks of adsorbed AEP-GO on the steel surface were visible even at the lowest concentration of 1 ppm (Fig. 5c) due to the silver nanoparticles'

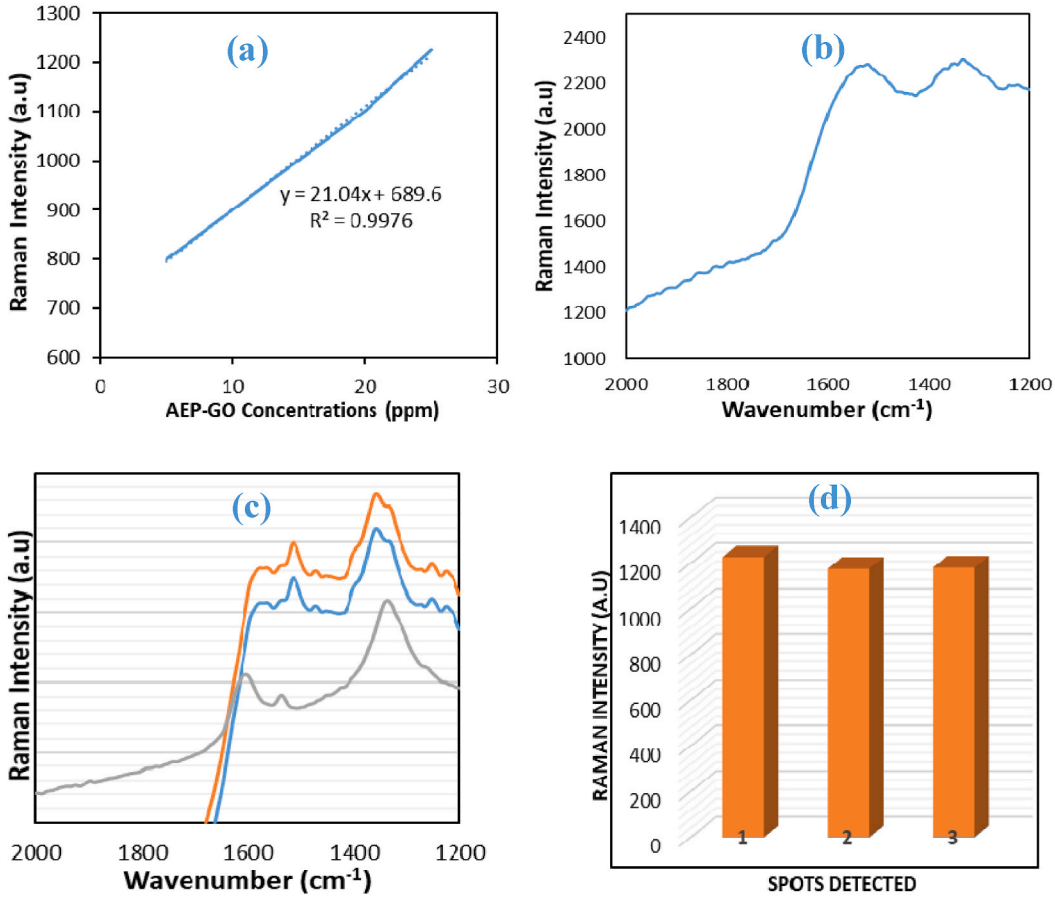


**Fig. 6.** (a) AEP-GO SERS intensities at 1320 $cm^{-1}$ as a function of concentrations (5–25 ppm), (b)SERS spectra of 25 ppm AEP-GO observed at three random spots of the SERS tape, (c) SERS spectrum of 1 ppm AEP-GO and (d) Raman intensity distribution at 1320 $cm^{-1}$ for 25 ppm of AEP-GO at three random spots of the SERS tape.

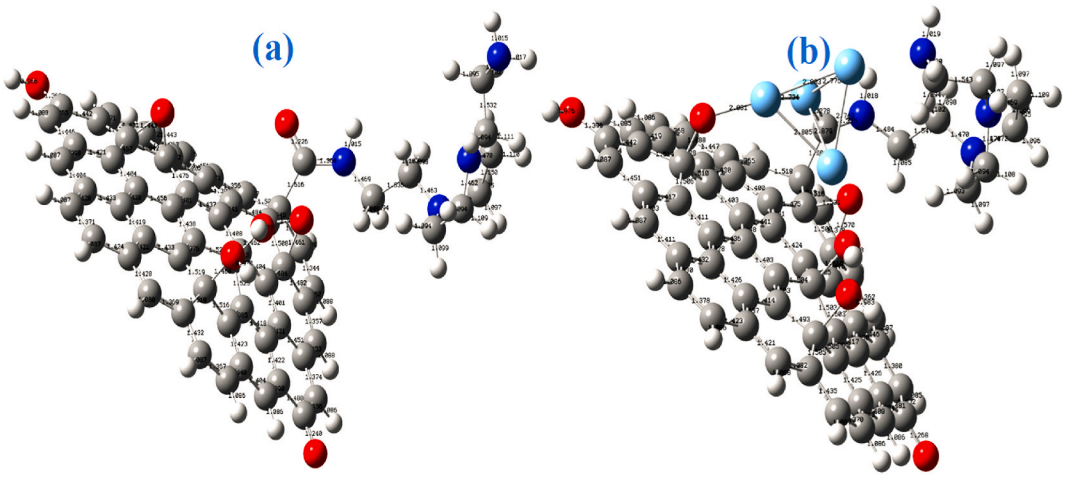


**Fig. 7.** Optimized structure of (a) AEP-GO and (b) AEP-GO_Ag adduct.

high electromagnetic field amplification. A linear correlation graph of SERS intensity against AEP-GO concentrations (5–25 ppm) (Fig. 6a) was plotted to assess the potential for quantitative detection of AEP-GO. A strong linear correlation with a coefficient of determination ($R^2$) of 0.9976 indicates that the SERS signal intensity increases as AEP-GO concentration increases. The SERS spectrum

of the 1 ppm AEP-GO shows a very visible signal with a signal-to-noise ratio far greater than 3 (Fig. 6b), suggesting the SERS sensor limits of detection (LOD) to be far lower than 1 ppm. Similarly, an LOD of 1.2 ppm was reported for the detection of benzotriazole adsorbed on the surface of aluminium alloy in 3.5 % NaCl in the presence of a SERS tape [33]. A lower LOD of 28.8 ng for the detection of pesticide residues from fruits and vegetables using transparent adhesive tapes and $Al_2O_3$-coated silver nanorods [39]. The enhancement of the adsorbed inhibitor signal is provided by the Plasmon resonance in the AgNPs [24]. This demonstrates the sensor's incredible detection capacity. To evaluate the AgNPs tape sensor's reproducibility, peak intensities at 1320 $cm^{-1}$ for 25 ppm AEP-GO from 3 randomly selected spots on the SERS tape were collected. The SERS spectra of the three randomly selected spots on the SERS tape for the 25 ppm AEP-GO are presented in Fig. 6c. There was only a very small intensity fluctuation (less than 3 %) that was seen (Fig. 6d). This is because of the consistency in the morphology and distribution of the AgNPs on the translucent tape. The even distribution of the AgNPs provides the SERS tape with its excellentsensitivity and consistency, enabling dependable analysis of corrosion inhibitors.

The characteristics Raman peaks increase with increasing concentrations of the inhibitor. This corroborated well with the weight loss and electrochemical results reported in our previous study [34]. The appearance of the characteristic Raman bands of the inhibitor compound on the SERS spectra, suggests the adsorption of the inhibitor molecules on the steel surface thereby blocking the steel surface from the aggressive acid attack.

### *3.3. AEP-GO - AgNPs interaction*

The optimized structure of the AEP-GO_Ag adduct shows that the silver metals approached the AEP-GO oxygen atom at the GO epoxy group rather than the oxygen atom at the carbonyl and the hydroxyl groups (Fig. 7b). This can be attributed to the lesser stability of the epoxy group as compared to the carbonyl and the hydroxyl groups. The epoxy two C–O bond distance in the AEP-GO is 1.443 Å. The bond distance increases to 1.488 Å in AEP-GO_Ag adduct, a consequence of the epoxy ring opening [40]. The calculated bond distance of Ag–O in AEP-GO_Ag adduct was 2.081 Å. The Ag–Ag bonds in AEP-GO_Ag adduct are 2.803, 2.776, 2.749, 2.879, 2.734, and 2.805 Å with a mean Ag–Ag bond angle of 2.791 Å close to the experiment mean value (2.850 Å) reported by Puyo et al. [41]. The computed bond distance between the AEP N-atom and the GO carboxyl C-atom is longer in AEP-GO (1.364 Å) (Fig. 7a) as compared to the AEP-GO_Ag adduct (1.355 Å) (Fig. 7b). This may be due to a secondary interaction between the other silver atoms in the silver cluster and the AEP-GO nitrogen atom on the other end [30].

## 4. Conclusion

Utilizing the surface-enhanced Raman scattering (SERS) technique, a silver nanoparticle-attached transparent tape sensor was employed to detect corrosion inhibitor (AEP-GO) on the carbon steel surface in this work. SERS detection revealed considerable amplification of inhibitor Raman signals on the carbon steel surface, which was used to study inhibitor adsorption behavior. According to the SERS analysis, the Raman signals of AEP-GO on the carbon surface steadily increase with increasing AEP-GO concentration in good agreement with the findings from our previous study [34]. DFT calculation predicted the silver metals to approach the AEP-GO oxygen atom at the GO epoxy group rather than the oxygen atom at the carbonyl and hydroxyl groups. Because of its versatility and lack of substrate material restrictions, the SERS tape created in this study can be utilized as a sensor to track corrosion inhibitors' dynamic adsorption irrespective of the metal type.

## CRediT authorship contribution statement

**Kabiru Haruna:** Conceptualization, Data curation, Investigation, Methodology, Writing – original draft, Writing – review & editing. **Tawfik A. Saleh:** Conceptualization, Project administration, Resources, Supervision, Writing – review & editing. **Ahmad A. Sorour:** Project administration, Resources.

## Declaration of competing interest

The authors declare that they have no known competing financial interests or personal relationships that could have appeared to influence the work reported in this paper.

## References

[1] K. Haruna, T. Saleh, M.A. Quraishi, Expired metformin drug as green corrosion inhibitor for simulated oil/gas well acidizing environment, J. Mol. Liq. 315 (2020), 113716, https://doi.org/10.1016/j.molliq.2020.113716.
[2] A.-R.I. Mohammed, M.M. Solomon, K. Haruna, S.A. Umoren, T.A. Saleh, Evaluation of the corrosion inhibition efficacy of Cola acuminata extract for low carbon steel in simulated acid pickling environment, Environ. Sci. Pollut. Res. (2020), https://doi.org/10.1007/s11356-020-09636-w.
[3] K. Haruna, T.A. Saleh, The inhibition performance of diaminoalkanes functionalized GOs against carbon steel corrosion in 15% HCl environment, Chem. Eng. J. 448 (2022), 137402, https://doi.org/10.1016/J.CEJ.2022.137402.
[4] T.A. Saleh, K. Haruna, B. Alharbi, Diaminoalkanes functionalized graphene oxide as corrosion inhibitors against carbon steel corrosion in simulated oil/gas well acidizing environment, J. Colloid Interface Sci. 630 (2023) 591–610, https://doi.org/10.1016/j.jcis.2022.10.054.
[5] K.A. Alamry, M.A. Hussein, A. Musa, K. Haruna, T.A. Saleh, The inhibition performance of a novel benzenesulfonamide-based benzoxazine compound in the corrosion of X60 carbon steel in an acidizing environment, RSC Adv. 11 (2021) 7078–7095, https://doi.org/10.1039/d0ra10317a.

[6] O. Olivares-Xometl, N.V. Likhanova, R. Martínez-Palou, M.A. Domínguez-Aguilar, Electrochemistry and XPS study of an imidazoline as corrosion inhibitor of mild steel in an acidic environment, Mater. Corros. 60 (2009) 14–21, https://doi.org/10.1002/maco.200805044.

[7] D.A. López, W.H. Schreiner, S.R. De Sánchez, S.N. Simison, The influence of carbon steel microstructure on corrosion layers: an XPS and SEM characterization, Appl. Surf. Sci. 207 (2003) 69–85, https://doi.org/10.1016/S0169-4332(02)01218-7.

[8] T.H. Hu, H.W. Shi, T. Wei, S.H. Fan, F.C. Liu, E.H. Han, Corrosion protection of AA2024-T3 by cerium malate and cerium malate-doped sol–gel coatings, Acta Metall. Sin. (English Lett. 32 (2019) 913–924, https://doi.org/10.1007/s40195-018-0846-x.

[9] I.B. Obot, N.K. Ankah, A.A. Sorour, Z.M. Gasem, K. Haruna, 8-Hydroxyquinoline as an alternative green and sustainable acidizing oilfield corrosion inhibitor, Sustain. Mater. Technol. (2017), https://doi.org/10.1016/j.susmat.2017.09.001.

[10] M.M. Solomon, S.A. Umoren, Enhanced corrosion inhibition effect of polypropylene glycol in the presence of iodide ions at mild steel/sulphuric acid interface, J. Environ. Chem. Eng. 3 (2015) 1812–1826, https://doi.org/10.1016/j.jece.2015.05.018.

[11] L.B. Coelho, D. Cossement, M.G. Olivier, Benzotriazole and cerium chloride as corrosion inhibitors for AA2024-T3: an EIS investigation supported by SVET and ToF-SIMS analysis, Corrosion Sci. 130 (2018) 177–189, https://doi.org/10.1016/j.corsci.2017.11.004.

[12] P. Visser, K. Marcoen, G.F. Trindade, M.L. Abel, J.F. Watts, T. Hauffman, J.M.C. Mol, H. Terryn, The chemical throwing power of lithium-based inhibitors from organic coatings on AA2024-T3, Corrosion Sci. 150 (2019) 194–206, https://doi.org/10.1016/j.corsci.2019.02.009.

[13] K. Haruna, T.A. Saleh, Graphene oxide with dopamine functionalization as corrosion inhibitor against sweet corrosion of X60 carbon steel under static and hydrodynamic flow systems, J. Electroanal. Chem. J. 920 (2022), 116589, https://doi.org/10.1016/j.jelechem.2022.116589.

[14] Y. Lei, N. Sheng, A. Hyono, M. Ueda, T. Ohtsuka, Influence of pH on the synthesis and properties of polypyrrole on copper from phytic acid solution for corrosion protection, Prog. Org. Coating 77 (2014) 774–784, https://doi.org/10.1016/j.porgcoat.2014.01.002.

[15] H. Shi, E.H. Han, S.V. Lamaka, M.L. Zheludkevich, F. Liu, M.G.S. Ferreira, Cerium cinnamate as an environmentally benign inhibitor pigment for epoxy coatings on AA 2024-T3, Prog. Org. Coating 77 (2014) 765–773, https://doi.org/10.1016/j.porgcoat.2014.01.003.

[16] I. Alessandri, J.R. Lombardi, Enhanced Raman scattering with dielectrics, Chem. Rev. 116 (2016) 14921–14981, https://doi.org/10.1021/acs.chemrev.6b00365.

[17] X. Zhang, Q.H. Tan, J. Bin Wu, W. Shi, P.H. Tan, Review on the Raman spectroscopy of different types of layered materials, Nanoscale 8 (2016) 6435–6450, https://doi.org/10.1039/c5nr07205k.

[18] L. Guerrini, R. Arenal, B. Mannini, F. Chiti, R. Pini, P. Matteini, R.A. Alvarez-Puebla, SERS detection of amyloid oligomers on metallorganic-decorated plasmonic beads, ACS Appl. Mater. Interfaces 7 (2015) 9420–9428, https://doi.org/10.1021/acsami.5b01056.

[19] R.S. Das, Y.K. Agrawal, Review Raman spectroscopy: recent advancements, techniques and applications, Vib. Spectrosc. 57 (2011) 163–176.

[20] K. Haruna, T.A. Saleh, M.K. Hossain, A.A. Al-Saadi, Hydroxylamine reduced silver colloid for naphthalene and phenanthrene detection using surface-enhanced Raman spectroscopy, Chem. Eng. J. 304 (2016) 141–148, https://doi.org/10.1016/j.cej.2016.06.050.

[21] H. Schmidt, N.B. Ha, J. Pfannkuche, H. Amann, H.-D. Kronfeldt, G. Kowalewska, Detection of PAHs in seawater using surface-enhanced Raman scattering (SERS), Mar. Pollut. Bull. 49 (2004) 229–234, https://doi.org/10.1016/j.marpolbul.2004.02.011.

[22] T. Murphy, S. Lucht, H. Schmidt, H.-D. Kronfeldt, Surface-enhanced Raman scattering SERS system for continuous measurements of chemicals in sea-water, J. Raman Spectrosc. 31 (2000) 943–948.

[23] S. Lucht, T. Murphy, H. Schmidt, H.-D. Kronfeldt, J Raman Spectroscopy - 2000 - lucht - Optimized recipe for sol gel-based SERS substrates.pdf, J. Raman Spectrosc. 31 (2000) 1017–1022.

[24] E.C. Le Ru, P.G. Etchegoin, Principles of Surface-Enhanced Raman Spectroscopy: and Related Plasmonic Effects, Elsevier B.V., 2009, https://doi.org/10.1016/B978-0-444-52779-0.X0001-3.

[25] H.F. Yang, J. Feng, Y.L. Liu, Y. Yang, Z.R. Zhang, G.L. Shen, R.Q. Yu, Electrochemical and surface enhanced Raman scattering spectroelectrochemical study of phytic acid on the silver electrode, J. Phys. Chem. B 108 (2004) 17412–17417, https://doi.org/10.1021/jp049739b.

[26] N. Pirhady Tavandashti, M. Ghorbani, A. Shojaei, J.M.C. Mol, H. Terryn, K. Baert, Y. Gonzalez-Garcia, Inhibitor-loaded conducting polymer capsules for active corrosion protection of coating defects, Corrosion Sci. 112 (2016) 138–149, https://doi.org/10.1016/j.corsci.2016.07.003.

[27] P. Song, S. Shen, C.C. Li, X.Y. Guo, Y. Wen, H.F. Yang, Insight in layer-by-layer assembly of cysteamine and l-cysteine on the copper surface by electrochemistry and Raman spectroscopy, Appl. Surf. Sci. 328 (2015) 86–94, https://doi.org/10.1016/j.apsusc.2014.12.015.

[28] P. Song, X.Y. Guo, Y.C. Pan, S. Shen, Y. Sun, Y. Wen, H.F. Yang, Insight in cysteamine adsorption behaviors on the copper surface by electrochemistry and Raman spectroscopy, Electrochim. Acta 89 (2013) 503–509, https://doi.org/10.1016/j.electacta.2012.11.096.

[29] H. Yang, X. Sun, J. Zhu, A. Ji, X. Ma, Z. Zhang, Surface enhanced Raman scattering, in situ spectro-electrochemical, and electrochemical impedance spectroscopic investigations of 2-amino-5-mercapto-1, 3,4-thiadiazole monolayers at a silver electrode, J. Phys. Chem. C 111 (2007) 7986–7991, https://doi.org/10.1021/jp070439e.

[30] S.G. Harroun, Y. Zhang, T.-H. Chen, C.-L. Hsu, H.-T. Chang, Adsorption orientation of 8-azaadenine on silver nanoparticles determined by SERS and DFT, J. Raman Spectrosc. 49 (2018), 1-376–382, http://journal.um-surabaya.ac.id/index.php/JKM/article/view/2203.

[31] E.F. Silva, J.S. Wysard, M.C.E. Bandeira, O.R. Mattos, Electrochemical and surface enhanced Raman spectroscopy study of Guanine as corrosion inhibitor for copper, Corrosion Sci. 191 (2021), 109714, https://doi.org/10.1016/j.corsci.2021.109714.

[32] E.F. Silva, M.C.E. Bandeira, W.A. Alves, O.R. Mattos, Surface-enhanced Raman scattering and electrochemical investigations on the adsorption of imidazole: imidazolium couple and its implications on copper corrosion inhibition, J. Electrochem. Soc. 165 (2018) C375–C384, https://doi.org/10.1149/2.0841807JES/XML.

[33] L. Ma, J. Wang, C. Ren, P. Ju, Y. Huang, F. Zhang, F. Zhao, Z. Zhang, D. Zhang, Detection of corrosion inhibitor adsorption via a surface-enhanced Raman spectroscopy (SERS) silver nanorods tape sensor, Sensors Actuators, B Chem. 321 (2020), 128617, https://doi.org/10.1016/j.snb.2020.128617.

[34] K. Haruna, T.A. Saleh, N,N′-Bis-(2-aminoethyl)piperazine functionalized graphene oxide (NAEP-GO) as an effective green corrosion inhibitor for simulated acidizing environment, J. Environ. Chem. Eng. 9 (2021), 104967, https://doi.org/10.1016/j.jece.2020.104967.

[35] N. Leopold, B. Lendl, A new method for fast preparation of highly surface-enhanced Raman scattering (SERS) active silver colloids at room temperature by reduction of silver nitrate with hydroxylamine hydrochloride, J. Phys. Chem. B 107 (2003) 5723–5727, https://doi.org/10.1021/jp027460u.

[36] D.J.F.M.J. Frisch, G.W. Trucks, H.B. Schlegel, G.E. Scuseria, M.A. Robb, J.R. Cheeseman, G. Scalmani, V. Barone, B. Mennucci, G.A. Petersson, H. Nakatsuji, M. Caricato, X. Li, H.P. Hratchian, A.F. Izmaylov, J. Bloino, G. Zheng, J.L. Sonnenberg, M. Had, Gaussian 09, 2009.

[37] I.B. Obot, K. Haruna, T.A. Saleh, Atomistic simulation: a unique and powerful computational tool for corrosion inhibition research, Arabian J. Sci. Eng. 44 (2019), https://doi.org/10.1007/s13369-018-3605-4.

[38] G. Mie, Beiträge zur Optik trüber Medien, speziell kolloidaler Metallösungen, Ann. Phys. 330 (1908) 377–445, https://doi.org/10.1002/andp.19083300302.

[39] J. Jiang, S. Zou, L. Ma, S. Wang, J. Liao, Z. Zhang, Surface-enhanced Raman scattering detection of pesticide residues using transparent adhesive Tapes and coated silver nanorods, ACS Appl. Mater. Interfaces 10 (2018) 9129–9135, https://doi.org/10.1021/acsami.7b18039.

[40] K. Dyduch, A. Roznowska, M. Srebro-hooper, B.Y. Lee, A. Michalak, Theoretical study on epoxide ring-opening in CO 2/epoxide copolymerization catalyzed by bifunctional salen-type cobalt (III) complexes : influence of stereoelectronic factors, Catalyst 11 (2021) 328.

[41] M. Puyo, E.L. Tailhades, L. Vendier, M.L. Kahn, P. Fau, K. Fajerwerg, C. Lepetit, Topological analysis of Ag – Ag and Ag – N interactions in silver amidinate precursor complexes of silver nanoparticles, Inorg. Chem. 59 (2020) 4328–4339.